Influence of Nickel Addition on the Stability, Trapping, and Diffusion Behaviour of Hydrogen in Vanadium: A First-Principles Investigation

Jiayao Qin
Guilin University of Electronic Technology
Zhigao Liu
Guilin University of Electronic Technology
Wei Zhao
South China University of Technology
Dianhui Wang
Guilin University of Electronic Technology
Yanli Zhang
Guilin University of Electronic Technology
Yan Zhong
Guilin University of Electronic Technology
Chaohao Hu
Guilin University of Electronic Technology
Zhongmin Wang (zmwang@guet.edu.cn)
Guilin University of Electronic Technology
Jiangwen Liu
South China University of Technology

Research Article

Keywords: Nickel substitution, Hydrogen trapping, Diffusion properties, Vanadium, First-principles calculation

Posted Date: January 13th, 2021

DOI: https://doi.org/10.21203/rs.3.rs-143116/v1

Influence of nickel addition on the stability, trapping, and diffusion behaviour of hydrogen in vanadium: A first-principles investigation

Jiayao Qin†[a, b], Zhigao Liu†[a], Wei Zhao [b], Dianhui Wang [a], Yanli Zhang [a],

Yan Zhong [a], Chaohao Hu [a], Zhongmin Wang [a, c *], Jiangwen Liu [b *]

a School of Materials Science and Engineering, Guangxi Key Laboratory of Information Materials, Guilin University of Electronic Technology, Guilin 541004, China.

b School of Materials Science and Engineering, Key Laboratory of Advanced Energy Storage Materials of Guangdong Province, South China University of Technology, Guangzhou 510640, China.

c College of Materials and Chemical Engineering, Hezhou University, Hezhou 542899, China

* Corresponding author.

E-mail addresses: zmwang@guet.edu.cn (Zhongmin Wang),

mejwliu@scut.edu.cn (Jiangwen Liu).

†These authors contributed equally to this work.

Abstract: Hydrogen embrittlement causes deterioration of materials used in hydrogen energy systems. Alloying is an effective means for overcoming this issue. In this study, the first-principles calculation method was used to investigate the effects of alloying Ni on the stability, dissolution, trapping, and diffusion behaviour of interstitial/vacancy H atoms in V. The calculated phonon spectra and solution energies of the vacancy/interstitial H atoms revealed that the V–Ni phase was dynamically and thermodynamically stable, and Ni addition could reduce the stability of V hydrides and improve their resistance to H embrittlement. H atoms in the interstitials and vacancies preferentially occupied the tetrahedral interstitial site (TIS) and octahedral interstitial site (OIS) with the lowest solution energies and diffused along the TIS → TIS and OIS → OIS paths with the minimum diffusion barrier energies. The trapping energy of the vacancy H atoms indicated that the addition of Ni could reduce the H trapping capability of the vacancies and suppress the retention of H in V. Detailed analysis of the calculated H diffusion barriers indicated that the presence of monovacancy defects blocked the diffusion of H atoms more than the presence of interstitials, and Ni doping did not enhance the H diffusion coefficient.

Keywords: Nickel substitution; Hydrogen trapping; Diffusion properties; Vanadium; First-principles calculation

Introduction

Hydrogen, a clean, efficient, and renewable fuel, is regarded as an indispensable energy source for the future owing to the gradual depletion of fossil fuels[1,2]. However, to develop hydrogen energy on a large scale, the breakthrough lies in understanding the interactions between hydrogen and materials, such as those related to H-storage and H embrittlement, which can decrease the mechanical properties of metallic materials[3,4,5]. Dense metallic membranes are applied in high-purity hydrogen separation from gaseous mixtures and are likely to form hydrides, especially at high hydrogen partial pressures, thus degrading the mechanical properties of these membranes[6,7]. Similarly, the structural materials used in fusion and fission reactors generate several hydrogen impurities and vacancies that result in

H bubble formation and blistering, embrittlement, and swellings, thus reducing the mechanical properties of plasma-facing materials[8,9,10].

V, an ideal hydrogen separation material, has the highest hydrogen permeability and costs lower than the current widely used Pd and its alloys[11,12,13]. Atomic hydrogen selectively diffuses through the Pd alloy membrane, yielding hydrogen with high purity (≥ 99.9999%) [6]. Low-activation V has also been identified as one of the most crucial first-wall and blanket materials for advanced fusion reactors because it has excellent resistance to neutron irradiation, superior high-temperature mechanical properties, and high compatibility with liquid lithium blankets[10,14,15]. V-based solid solution hydrogen storage alloys with a body-centred cubic structure are capable of absorbing/desorbing hydrogen fast at room temperature and have higher capacities than that of pure V. They have a theoretical hydrogen uptake of 3.8% (mass fraction), higher than the uptakes of the AB5- (1.4%) and AB-type (1.86%) hydrogen storage alloys. Consequently, solid solution hydrogen storage alloys could be considered new potential materials for vehicle hydrogen storage systems[16,17]. In such applications, the formed stable V hydride is a brittle phase and often becomes the source of fracture under the action of external forces[13]. Additionally, because of the occurrence of substantial vacancy defects, H bubbles are easily formed. This considerably affects the stability of the structural defects in the metal lattice and the mobility of H, leading to brittle fracture of pure V[14]. H embrittlement is a key problem that restricts the practical applications of V-based alloy materials.

Alloying is one of the effective ways to solve this problem, leading to improvements in several properties of these materials[18,19,20]. More specifically, decreased hydrogen solubility and restrained hydride formation are desirable. Experimental studies have shown that hydrogen solubility in transition metal alloys exhibits the following sequence: V–Ti > V–Cr > V–Mn > V–Fe > V–Co > V–Ni [13,15]; adding Ni to V substantially reduces the hydrogen solubility of pure V, improving its resistance to H embrittlement[21,22,23]. Further, Ni, an effective catalytic component, is widely employed in hydrogen storage materials, chemical fuels, and organic chemical synthesis[24,25]. Moreover, the V–Ni binary alloy system is

extensively studied owing to its high hydrogen permeability and mechanical strength[26,27]. Several studies involving density functional theory (DFT) calculations have reported that alloying V with transition metals can decrease its H solubility and embrittlement and enhance the H diffusion coefficient[26,27,28,29]. However, the vacancy defect mechanism has not been investigated sufficiently. Until now, few studies have examined the fundamental mechanism of Ni substitution in transition metals and its effect on the interaction between V monovacancies and miscellaneous H atoms. The complex mechanism of the interaction between H and V vacancies has not been elucidated. Therefore, it is extremely significant to theoretically examine the influence of Ni addition on the stability and diffusion behaviours of interstitial and vacancy H atoms and the trapping of multiple H atoms in the vacancies.

Therefore, to address the abovementioned issues, the formation energies of interstitial H, vacancy H, and H-vacancy clusters were determined using a highly accurate first-principles calculation method in this study. We comprehensively researched the stabilities, dissolution, trapping, and diffusion behaviour of H atoms in interstitial positions and vacancies, along with the influence of Ni substitution. We expect that the findings of this study will serve as a valuable reference for the industrial development of H-storage, H-separation, reactor first-wall, and blanket systems using V-based alloys, which are promising candidate materials for these applications.

Methods

First-principles calculations based on DFT were conducted using the Vienna Ab initio Simulation Package[30,31]. The generalised gradient approximation with the Perdew–Burke–Ernzerhof forms for the exchange-correlation interaction and the projected augmented wave methods for the core-electron interaction were used[32,33,34]. A 54-atom supercell containing a 3 × 3 × 3 unit cell was used. The V 3d3 4s2, Ni 3d8 4s2, and H 1s1 electrons were regarded as the valence electrons. A kinetic cut-off energy of 360 eV and *k*-meshes with dimensions of 4 × 4 × 4 were applied. While optimising the supercell size, shape, and atomic positions, the convergence threshold for the self-consistency energy was less than 1×10^{-6} eV atom^{-1}, and

the force acting on each atom was less than the maximum of 1×10^{-2} eV Å^{-1}. The optimum diffusion paths and energy barriers of H atoms between the initial and final configurations were calculated by employing the extremely well-known climbing-image nudged-elastic-band (CI-NEB) method[35]. The phonon spectra and thermodynamic properties were calculated using the PHONOPY code[36].

The solution energy of an interstitial (vacancy) H atom for a metal or alloy is defined as follows[14]:

$$E_{sol}(H) = E(VNiH) - E(VNi) - \frac{1}{2}E(H_2) \quad (1)$$

The vacancy formation energy is calculated as follows[10]:

$$E_f(vac) = E(vac) - \frac{N-2}{N}E(V) - E(Ni) \quad (2)$$

Here, E(VNiH), E(VNi), E(V), E(Ni), E(H_2), and E(vac) concretely represent the total energies of the respective systems; N is the number of V atoms.

There are two ways to trap H atoms in vacancies, namely trapping them simultaneously and sequentially (one by one). Hence, the trapping energies associated with these two different trapping methods should be defined separately[37]. The average trapping energy of each H atom trapped simultaneously is defined as

$$E_{trap}(sim) = \frac{1}{n}(E_{vac+nH} - E_{vac}) - \frac{1}{n}\left(nE_{V,H(TIS)} - E_V\right). \quad (3)$$

The H atoms are sequentially placed in the monovacancy, and the trapping energy of each H atom is given as

$$E_{trap}(seq) = (E_{vac+nH} - E_{vac+(n-1)H}) - (E_{V,H(TIS)} - E_V), \quad (4)$$

where $E_{\mathrm{vac}+n\mathrm{H}}$ and $E_{\mathrm{vac}+(n\text{-}1)\mathrm{H}}$ are the total energies of n H atoms and (n-1) H atoms in the vacancy of the system, respectively, and $E_{\mathrm{V,H(TIS)}}$ refers to the total energy of the H atoms in the tetrahedral interstitial site (TIS).

According to the statistical method described by Maroevic et al.[38] and Rao et al.[39], the vacancy concentration can be written as

$$C(vac) = \sum_{n=0}^{z} \frac{z!}{(z-n)!n!} \left(\frac{n_H}{\beta N}\right)^n \left(1 - \frac{n_H}{\beta N}\right)^{z-n} \frac{1}{1+\exp\left(\frac{E_f+\Delta\varepsilon}{kT}\right)}. \quad (5)$$

In the above formula, *z, n, β, n_H/N, k, T, E_f, and Δε* are the maximum number of trapped H atoms, number of H atoms, number of interstitial sites, H concentration, Boltzmann constant, temperature, vacancy formation energy, and H atom trapping energy, respectively.

Results

To determine the accuracy of our calculations, we calculated the stability of H atoms in V at the interstitial sites (TIS, diagonal interstitial site (DIS), and octahedral interstitial site (OIS)) and substitution site (SS), as plotted in Fig. 1(a). The solution energies of the H atoms were calculated to be −0.371, −0.336, −0.228, and +0.165 eV for the TIS, DIS, OIS, and SS, respectively. Apparently, the most favourable locations for H are the interstitial sites, and our calculation results are similar to the early experimental results that stated that the heat of solution is −0.36±0.3 eV[40]. In addition, the theoretical values of the solution energies reported by Luo[41] after the structural relaxation processes for TIS, OIS, and SS are −0.374, −0.226, and +1.83 eV, respectively. Furthermore, our calculations showed that the formation energy of the V vacancy is +2.473 eV, which agrees with the experimental value of 2.2±0.4 eV[42].

3.1. Influence of Ni substitution on structural stability of V

To examine the influence of Ni substitution on the structural stability of metallic V, we employed the density functional perturbation theory to optimise the linear response function and lattice dynamics matrix of a 2 × 2 × 2 body-centred cubic (bcc) supercell containing 15 V atoms and 1 Ni atom to calculate the phonon dispersion and phonon state density. The obtained phonon density of states was then used to calculate the thermal

properties. As shown in Fig. 1(b), there are 48 branches in the phonon spectrum, and each branch corresponds to a vibration mode; among these branches, 3 branches with low frequencies correspond to acoustic phonons and 45 branches with high frequencies correspond to optical phonons. The calculated phonon spectrum of the V–Ni binary alloy has no imaginary frequency, so the structure exhibits dynamical stability. Fig. 1(c) shows the phonon density of states in the bcc phase of V–Ni, including the total density of states and partial density of states. The V–Ni peak is at approximately 8 THz, whereas that of Ni occurs at 5.2 THz. Fig. 1(d) clearly shows the relationship between the thermodynamic properties and temperature. As the temperature increases, the vibrational free energy (F) decreases, whereas the entropy (S) increases. Moreover, the specific heat at constant volume (Cv) increases rapidly first and then gradually achieves a stable value. These changes were attributed to the lattice thermal vibration and electron heat capacity. In contrast, the internal energy (E) of the V–Ni crystals increases significantly with increasing temperatures, eventually which is proportional to the temperature.

According to the above analysis results, the H atom at TIS is energetically favourable; thus, it is necessary to further elucidate the interaction between H and Ni atoms. Fig. 2. shows the solution energies of H as functions of the Ni–H distances. The distance between the H atom and nearest-neighbour (1NN) Ni atom at TIS is 1.632 Å and the corresponding solution energy is −0.2 eV. This is higher than that (−0.33 eV to −0.37 eV) for Ni–H distances ranging from 2.728 Å to 6.565 Å, and it is also considerably higher than that in pure V, i.e. −0.371 eV. Interestingly, as the Ni–H distance increased from 1.632 to 2.728 Å, the H solution energy declined sharply to 0.33 eV. It remained almost unchanged and finally decreased when the Ni–H distance increased from 4.536 Å to 6.565 Å. However, it is worth mentioning that the effect of Ni substitution on the solubility of H is highly local, limited largely to within the Ni–H distances. Therefore, Ni substitution could significantly weaken the interaction between the V and H atoms and enhance the H solution energy, thus further improving the resistance of V to H embrittlement.

3.2. Stability of H atoms near multiple Ni atoms

We next investigated the H solution properties in TIS and OIS, which are composed of multiple (n = 1–6) Ni atoms. The H atom was placed in the TIS and OIS, and Ni atoms replaced its nearest neighbouring V atoms. A series of possible structure models were tested; finally, the most stable configurations were obtained, as shown in Fig. 3; the corresponding H solution energies are summarised in Fig. 4. Clearly, the highest solution energy for H atoms in TIS near two Ni atoms is −0.090 eV, and it gradually decreases as the number of nearest Ni atoms increases. The solution energies in all the cases exceeded −0.371 eV, i.e., the H solution energy in pure V. Meanwhile, the solution energies of H atoms at OIS increased significantly from −0.347 eV to −0.056 eV, indicating that Ni substitution could effectively reduce the stability of the V hydride formed, thus inhibiting H embrittlement of the material.

3.3. Interactions between monovacancy and multiple H atoms

Vacancy defects are one of the common point defects occurring in metals and alloys. We investigated the influence of introducing Ni as the substituent element on the stability of the monovacancies in V. By analysing the monovacancy defects around Ni atoms in V, we obtained three structural models, namely 1NN, 2NN, and 3NN sites, using a single vacancy as the reference site, as shown in Fig. 5. The formation energy of the 2NN (1.515 eV) site was lower than those of the 1NN (1.750 eV) and 3NN sites (1.904 eV). Thus, the 2NN site in the V–Ni alloy shows the best thermodynamic stability, and it was applied to investigate the interaction between multiple H atoms and a vacancy.

To investigate the interaction between multiple H atoms and a monovacancy, we first calculated the energetic stability of multiple H atoms at a monovacancy in V. The solution energies of multiple H atoms at the most suitable sites are summarised in Fig. 6(a). The H atoms in the V monovacancy occupy OIS (with a solution energy of −0.694 eV) instead of TIS and central sites. The corresponding numerical results show excellent agreement with those reported by Pengbo et al.[14]. As the number of H atoms increases, the solution energies gradually continue to decrease, indicating that the presence of multiple H atoms at a monovacancy is favourable for forming metal hydrides, thus leading to H embrittlement of

the material. Subsequently, the trapping energies of multiple H atoms were calculated, and they are presented in Fig. 6(b). The sequential trapping energy calculation results indicated that as many as six H atoms were trapped sequentially in a V monovacancy and were separately situated close to six OISs. Moreover, the presence of more than six H atoms is energetically unfavourable, which is in accordance with the early experimental results reported by Myers[43]. Six H atoms can become trapped at the nearest neighbouring OIS in a bcc metal monovacancy. The calculated simultaneous trapping energy results showed that at least eight H atoms could be trapped, and the H atom in the stable OIS started to shift towards the TIS when the number of H atoms exceeded six. However, Gui et al.[37] reported that a monovacancy in V can trap a maximum of 12 H atoms simultaneously based on first-principles calculations.

We calculated all the possible configurations involving multiple H atoms when an Ni atom is added. As shown in Fig. 6(c), the corresponding solution energies decrease gradually as the number of H atoms increases, indicating that the stability of H in the vacancy is stronger and the solubility of H involves an exothermic process. For comparison, the solution energies of multiple H atoms in the bulk V monovacancy before and after Ni addition are presented in Fig. 6(d). After adding Ni, the stability of V hydrides decreased, thereby inhibiting their H embrittlement. Fig. 6(e, f) present the trapping energies as functions of the H atom number. Obviously, the trapping energies of two–five H atoms sequentially or simultaneously trapped in the V–Ni monovacancy are lower than those of the corresponding V monovacancy. However, the trapped six H atoms exhibited very poor affinity towards the monovacancy, with simultaneous trapping energies of −0.003 eV, thereby indicating effective suppression of the H retention. Therefore, from the perspective of the trapping energy, the V–Ni monovacancy can capture up to six H atoms.

3.4. Monovacancy and Vac-*n*H cluster concentrations

To study the equilibrium concentrations of vacancies, we employed a statistical method[38,39] to estimate the intrinsic vacancy and Vac-*n*H cluster concentrations. The calculation results are presented in Fig. 7. As observed in Fig. 7(a, b), the concentrations of V

and V–Ni vacancies gradually increase with the increase in temperature, which means that the vacancy concentration can easily damage metals or alloys at high temperatures. As for the Vac-*n*H cluster concentration shown in Fig. 7(c, d), when the H/M ratio (H concentration) gradually increases at an operating temperature of 673 K, the Vac-*n*H cluster concentration also increases accordingly, thus proving that a high Vac-*n*H cluster concentration leads to H embrittlement. This finding is consistent with the observations of Matsumoto[44], who proved experimentally that sample cracking occurred when the H concentration in a V-based alloy exceeded C (H/M) = 0.2. The concentrations of the monovacancy and Vac-*n*H cluster in Ni-substituted V increased rapidly; however, the concentrations of V and V–Ni monovacancies were 7.675×10^{-32} and 8.679×10^{-20} at 400 K, respectively.

3.5. H diffusion in interstitials and vacancies

To further study the influence of Ni substitution on the H atom diffusion in interstitials and vacancies, we calculated the possible diffusion paths and migration energy barriers of H diffusion using the CI-NEB method[35], as shown in Fig. 8. However, we only considered the H atom diffusion between the most stable absorption sites. Based on our previous work[45], the diffusion energy barriers of H in perfect bulk V from TIS to TIS and TIS to OIS are 0.132 and 0.20 eV, respectively, indicating that the optimal diffusion paths are located between TISs (TIS → TIS). The calculated energy barriers for H are 0.711 and 1.120 eV from OIS to OIS and from OIS to the vacancy centre, respectively, when a monovacancy defect occurs in pure V, as seen in Fig. 8(a), suggesting that the H atom in the vacancy easily diffuses along the OIS → OIS path with the most favourable energetic state. Compared with the vacancy diffusion energy barriers, the H atom prefers migrating to interstitials because it only needs to overcome a small energy barrier.

After adding Ni atoms, as illustrated in Fig. 8(b), the H atom in the vacancy migrated from one OIS to another nearest neighbouring (1NN) OIS through various possible diffusion paths, with each path passing through an intermediate transition state. The computed energy barriers along paths a, b, c, d, and e were 0.994, 0.761, 0.792, 0.940, and 1.133 eV, respectively; thus, the optimal path for H diffusion is path b. Furthermore, we simulated the

diffusion behaviour of interstitial H, as depicted in Fig. 8(c). The H atom jumps from the first TIS on the left to the last TIS and moves closer to the Ni atoms in the middle with a low energy barrier of 0.288 eV, whereas the other paths have extremely high energy barriers, especially paths b and d. From a kinetic perspective, when the H atom gradually migrates to the TIS near the Ni atom (a → b → c → d → e: 5NN TIS diffusing to 1NN TIS), the H migration barrier tends to first increase and then decrease. The addition of Ni atoms does not reduce the H diffusion energy barrier compared with that observed in pure V; this could be attributed to the elastic effects and electronic properties of Ni[26]. In addition, the H atom constrained in the inner cavity of the vacancy needs to overcome the high energy barrier to escape from it. Therefore, the presence of Ni could control the nucleation and blistering of H in V.

Discussion

We investigated the influence of adding Ni on the stability, dissolution, trapping, and diffusion properties of H atoms in V using first-principles DFT calculations. The calculation results showed that the monovacancy formation energies of V and V–Ni were +2.473 and +1.515 eV, respectively. Single H atoms in interstitials and vacancies preferred to occupy TIS and OIS, respectively, owing to their low solution energy, and diffuse along the TIS → TIS and OIS → OIS paths with low energy barriers. H diffusion preferentially occurred in the interstitial sites rather than in the vacancies that were stronger traps for H atoms. Adding Ni could reduce H solubility and inhibit H retention to a certain extent and provide more diffusion paths. The monovacancy and Vac-*n*H cluster concentrations depend on the temperature and H concentration over a wide range. This study is helpful in understanding the interactions between H atoms and vacancy defects. This understanding provides insights into the trapping of multiple H atoms or the formation of H bubbles during H permeation, thus laying a theoretical foundation for the designing membrane materials from alloys.

Data availability

The datasets generated and analyzed during the current study are available from the corresponding author on reasonable request.

References

[1] Thomas, J. M., Edwards, P. P., Dobson, P. J. & Owen, G. P. Decarbonising energy: The developing international activity in hydrogen technologies and fuel cells. *J. Energy Chem.* **51**, 405-415 (2020).

[2] Yartys, V. A., Baricco, M., Colbe, J. B. V., Blanchard, D. & Zlotea, C. Materials for hydrogen-based energy storage: past, recent progress and future outlook. *J. Alloys Compd*. **827**, 153548 (2020).

[3] Lu, G. & Kaxiras, E. Hydrogen embrittlement of aluminum: the crucial role of vacancies. *Phys. Rev. Lett.* **94**, 155501 (2005).

[4] Abe, J. O., Popoola, A. P. I., Ajenifuja, E. & Popoola, O. M. Hydrogen energy, economy and storage: review and recommendation. *Int. J. Hydrog. Energy* **44**, 15072-15086 (2019).

[5] Xing, W. W. et al. First-principles study of hydrogen trapping behavior in face centered cubic metals (M=Ni, Cu and Al) with monovacancy. *Int. J. Hydrog. Energy* **45**, 25555-25566 (2020).

[6] Al-Mufachi, N. A., Rees, N. V. & Steinberger-Wilkens, R. Hydrogen selective membranes: a review of palladium-based dense metal membranes. *Renew. Sust. Energ. Rev*. **47**, 540-551 (2015).

[7] Yun, S. & Oyama, S. T. Correlations in palladium membranes for hydrogen separation: A review. *J. Membr. Sci.* **375**, 28-45 (2011).

[8] Li, X. T., Tang, X. Z., Fan, Y. & Guo, Y. F. The interstitial emission mechanism in a vanadium-based alloy. *J. Nucl. Mater.* **533**, 152121 (2020).

[9] Yang, Y. C. et al. Atomistic understanding of helium behaviors at grain boundaries in vanadium. *Comp. Mater. Sci.* **158**, 296-306 (2019).

[10] Hua, J. et al. Effects of Cr on H and He trapping and vacancy complexes in V in a fusion environment: A first-principles study. *Eur. Phys. J. B.* **90**, 119 (2017).

[11] Dolan, M. D. Non-Pd, BCC alloy membranes for industrial hydrogen separation. *J. Membr. Sci.* **362**, 12–28 (2010).

[12] Peng, J., Song, G. S., Daniel, L., Wu, W. P. & Hua, T. S. Vanadium-Based Alloy Membranes for Hydrogen Purification. *Rare Metal Mat. Eng*. **03**, 285-291 (2017).

[13] Phair, J. W. & Donelson, R. Developments and design of novel (Non-Palladium-Based) metal membranes for hydrogen separation. *Ind. Eng. Chem. Res.* **16**, 5657-74 (2006).

[14] Zhang, P. B. et al. Trapping of multiple hydrogen atoms in a vanadium monovacancy: A first-principles study. *J. Nucl. Mater*. **429**, 216-220 (2012).
[15] Zhang, P. B. et al. First principles investigations of hydrogen interaction with vacancy-oxygen complexes in vanadium alloys. *Int. J. Hydrog. Energy* **44**, 26637-26645 (2019).
[16] Li, D. et al. Research Progress of Vanadium-based Hydrogen Storage Alloy. *Mater. Rep*. **29**, 92-97 (2015).
[17] Kumar, S., Jain, A., Ichikawa, T., Kojima, Y. & Dey, G. K. Development of vanadium based hydrogen storage material: a review. *Renew. Sust. Energ. Rev*. **72**, 791-800 (2017).
[18] Yukawa, H. et al. Alloying effects on the hydriding properties of vanadium at low hydrogen pressures. *J. Alloys Compd.* **337**, 264-268 (2002).
[19]Kim, K. H., Shim, J. H. & Lee, B. J. Effect of alloying elements (Al, Co, Fe, Ni) on the solubility of hydrogen in vanadium: a thermodynamic calculation. *Int. J. Hydrog. Energy* **9**, 7836-7847 (2012).
[20] Dolan, M. D., Kellam, M. E., Mclennan, K. G., Liang, D. & Song, G. Hydrogen transport properties of several vanadium-based binary alloys. *Int. J. Hydrog. Energy* **23**, 9794-9799 (2013).
[21] Amano, M., Komaki, M. & Nishimura, C. Hydrogen permeation characteristics of palladium-plated V-Ni alloy membranes. *J. Less-Common Met*. **172**, 727-731 (1991).
[22] Nishimura, C., Komaki, M. & Amano, M. Hydrogen permeation characteristics of vanadium-nickel alloys . *Mater. Trans.* **32**, 501 (1991).
[23] Jiang, P. et al. Effect of partial Ni substitution in V85Ni15 by Ti on microstructure, mechanical properties and hydrogen permeability of V-based bcc alloy membranes. *Mater. Res. Express* **7**, 066505 (2020).
[24] Rusman, N. A. A. & Dahari, M. A review on the current progress of metal hydrides material for solid-state hydrogen storage applications. *Int. J. Hydrog. Energy* **41**, 12108-12126 (2016).
[25] Fan, K. et al. Nicke-vanadium monolayer double hydroxide for efficient electrochemical water oxidation. *Nat. Commun*. **7**, 11981 (2016).
[26] Qin, J. Y. et al. First-principle investigation of hydrogen solubility and diffusivity in transition metal-doped vanadium membranes and their mechanical properties. *J. Alloy Compd.* **805**, 747-756 (2019).
[27] Zhang, P. B. et al. Diffusion and retention of hydrogen in vanadium in presence of Ti and Cr: First-principles investigations. *J. Nucl. Mater.* **484**, 276-282 (2016).
[28] Lee, Y. S. et al. Role of alloying elements in vanadium-based binary alloy membranes for hydrogen separation. *J. Membr. Sci.* **51**, 332-341 (2012).
[29] Wang, Z. M. et al. Theoretical investigation of molybdenum/tungsten-vanadium solid

solution alloy membranes: thermodynamic stability and hydrogen permeation. *J. Membr. Sci.* **608**, 118200 (2020).

[30] Kresse, G. & Hafner, J. Ab-initio molecular dynamics for liquid metals. *Phys. Rev. B* **47**, 558-561 (1993).

[31] Kresse, G. & Furthmüller, J. Efficient iterative schemes for ab initio total-energy calculations using a plane-wave basis set. *Phys. Rev. B* **54**, 11169-11186 (1996).

[32] Perdew, J. P. & Wang Y. Accurate and simple analytic representation of the electron-gas correlation energy. *Phys. Rev. B* **45**, 13244-13249 (1992).

[33] löchl, P. E. Projector augmented-wave method. *Phys. Rev. B* **50**, 17953-17979 (1994).

[34] Perdew, J. P., Burke, K. & Ernzerhof, M. Generalized gradient approximation made simple. *Phys. Rev. Lett.* **77**, 3865-3868 (1998).

[35] Henkelman, G., Uberuaga, B. P. & Jonsson H. A climbing image nudged elastic band method for finding saddle points and minimum energy paths. *J. Chem. Phys.* **113**, 9901-9904 (2000).

[36] Togo, A. & Tanaka, I. First principles phonon calculations in materials science. *Scripta Mater.* **108**, 1-5 (2015).

[37] Gui, L. J. et al. First-principles investigation on vacancy trapping behaviors of hydrogen in vanadium. *J. Nucl. Mater.* **442**, S688-S693 (2013).

[38] Maroevic, P. & Mclellan, R. B. Equilibrium vacancy concentration in Pd–H solid solutions. *Acta Mater*. **46**, 5593-5597 (1998).

[39] Rao, J. P. et al. Vacancy and H Interactions in Nb. *Chin. Phys. Lett.* **28**, 127101-127104 (2011).

[40] Zhang, P., Zou, T., Liu, W., Yin, Y. & Zhao, J. Stability of X-C-vacancy complexes (X=H, He) in vanadium from first principles investigations. *J. Nucl. Mater*. **505**, 119-126 (2018).

[41] Luo, J. et al. Dissolution, diffusion and permeation behavior of hydrogen in vanadium: a first-principles investigation. *J. Phys. Condens. Matter* **23**, 135501(2011).

[42] Janot, C., George, B. & Delcroix, P. Point defects in vanadium investigated by mossbauer spectroscopy and positron annihilation. *J. Phys. F: Metal Phys*. **12**, 47-57 (1982).

[43] Myers, S. M., Richards, P. M., Wampler, W. R. & Besenbacher, F. Ion-beam studies of hydrogen-metal interactions. *J. Nucl. Mater.* **165**, 9-64 (1989).

[44] Matsumoto, Y., Yukawa, H. & Nambu, T. Quantitative evaluation of hydrogen embrittlement of metal membrane defected by in-situ small punch test under hydrogen permeation. *Metall. J. LXIII*. **63**, 74-78 (2010).

[45] Qin, J. Y. et al. Investigation of adsorption, dissociation, and diffusion properties of hydrogen on the V (100) surface and in the bulk: a first-principles calculation. *J. Adv. Res*. **21**, 25-34 (2020).

Acknowledgements

This work was financially supported by the National Natural Science Foundation of China (Nos. 51961010 and 5187010153) and Guangxi Science and Technology Project (GuiKeAB182810103).

Author contributions

Z.M.W., J.W.L. and C.H.H. conceived the study. J.Y.Q., Z.G.L. and D.H.W. carried out the numerical calculations. W.Z., Y.L.Z. and Y.Z. gave some comments. J.Y.Q. and Z.G.L. wrote the manuscript. All the authors contributed to the analysis and discussion of the results.

Competing interests

The authors declare no competing interests.

Figure legends

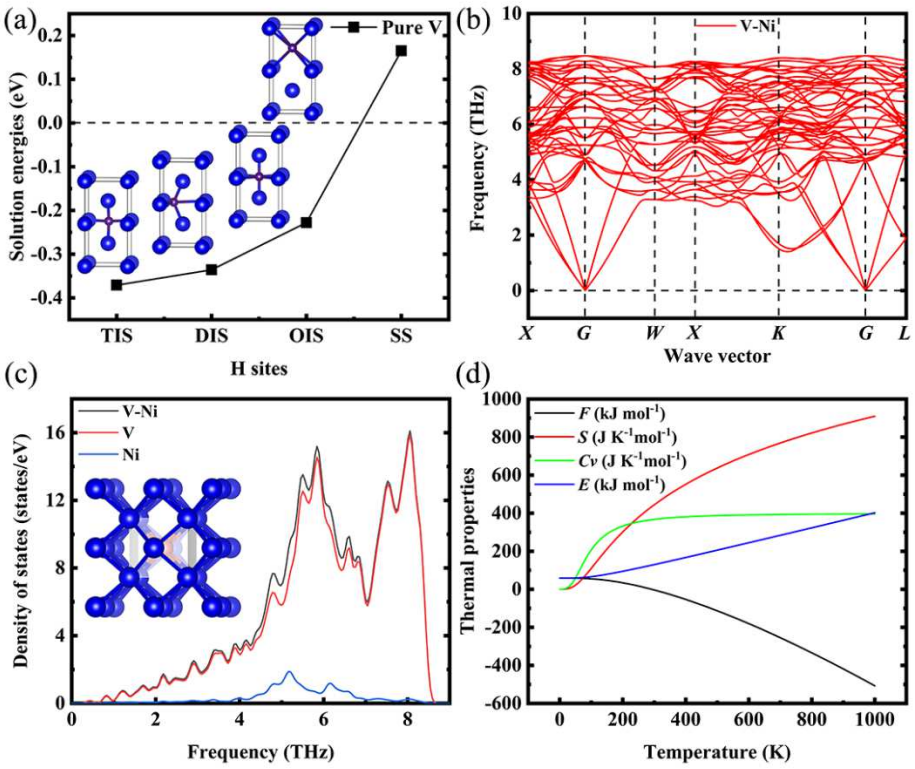

Fig. 1. (a) Solution energies of H atoms in interstitial and substitution sites of pure V and (b–d) phonon spectra and thermal properties of V–Ni. The blue, red, and purple spheres denote the V, Ni, and H atoms, respectively.

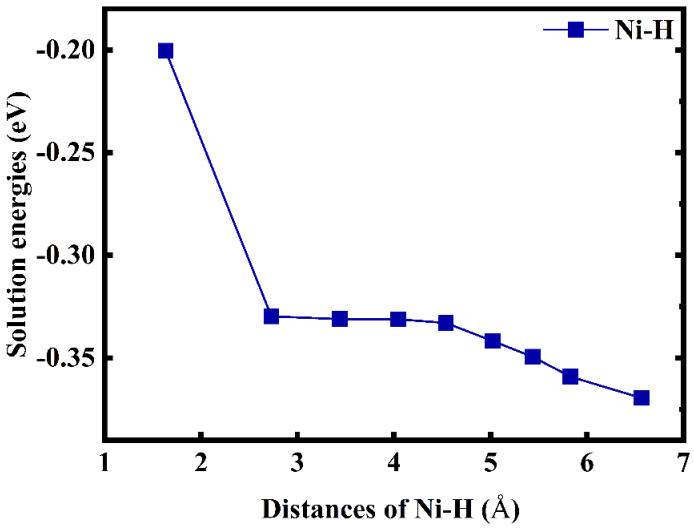

Fig. 2. Solution energies of H atoms with respect to the Ni–H distances in the TIS of V–Ni alloys.

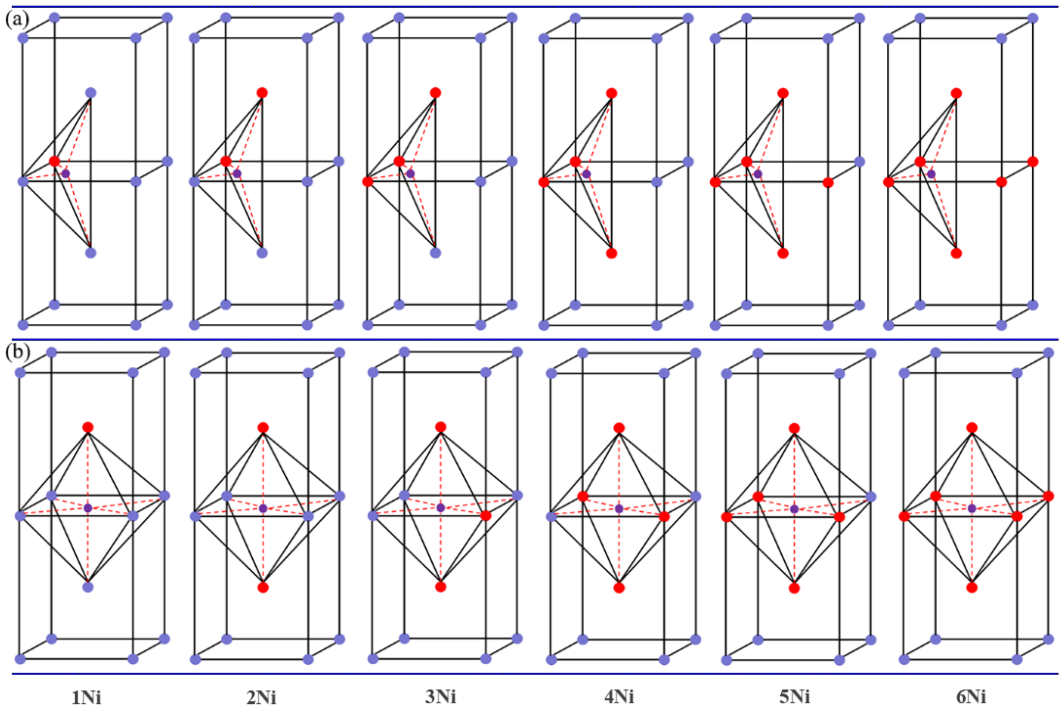

Fig. 3. Models demonstrating the substitution of V atoms by different numbers of Ni atoms at the (a) TIS and (b) OIS.

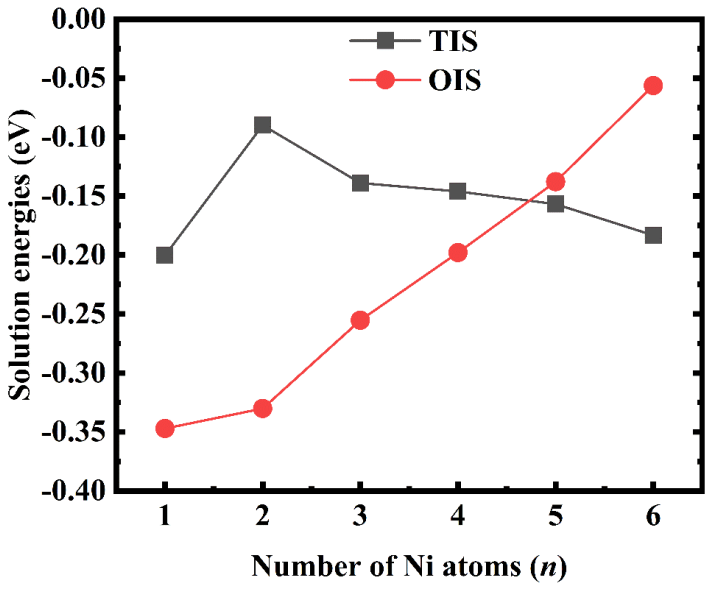

Fig. 4. Solution energies of one H atom at the TIS and OIS near (n = 1–6) Ni atoms.

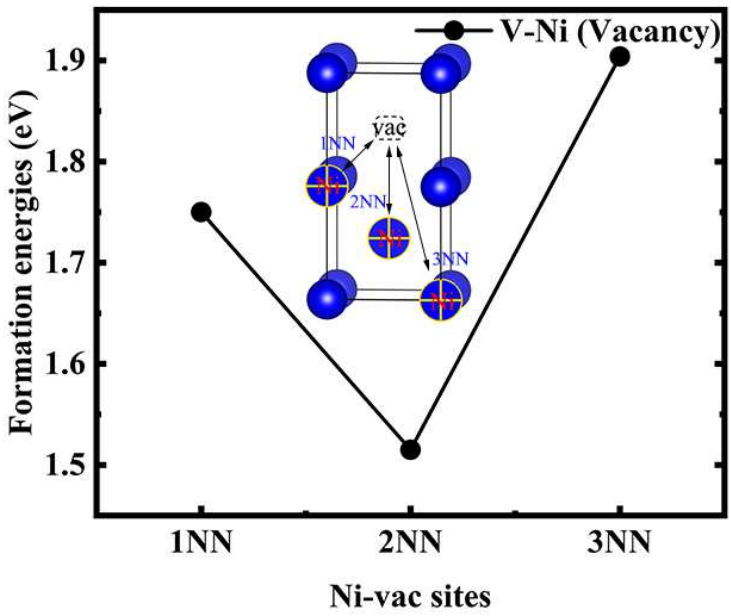

Fig. 5. Monovacancy formation energies in the V–Ni alloy.

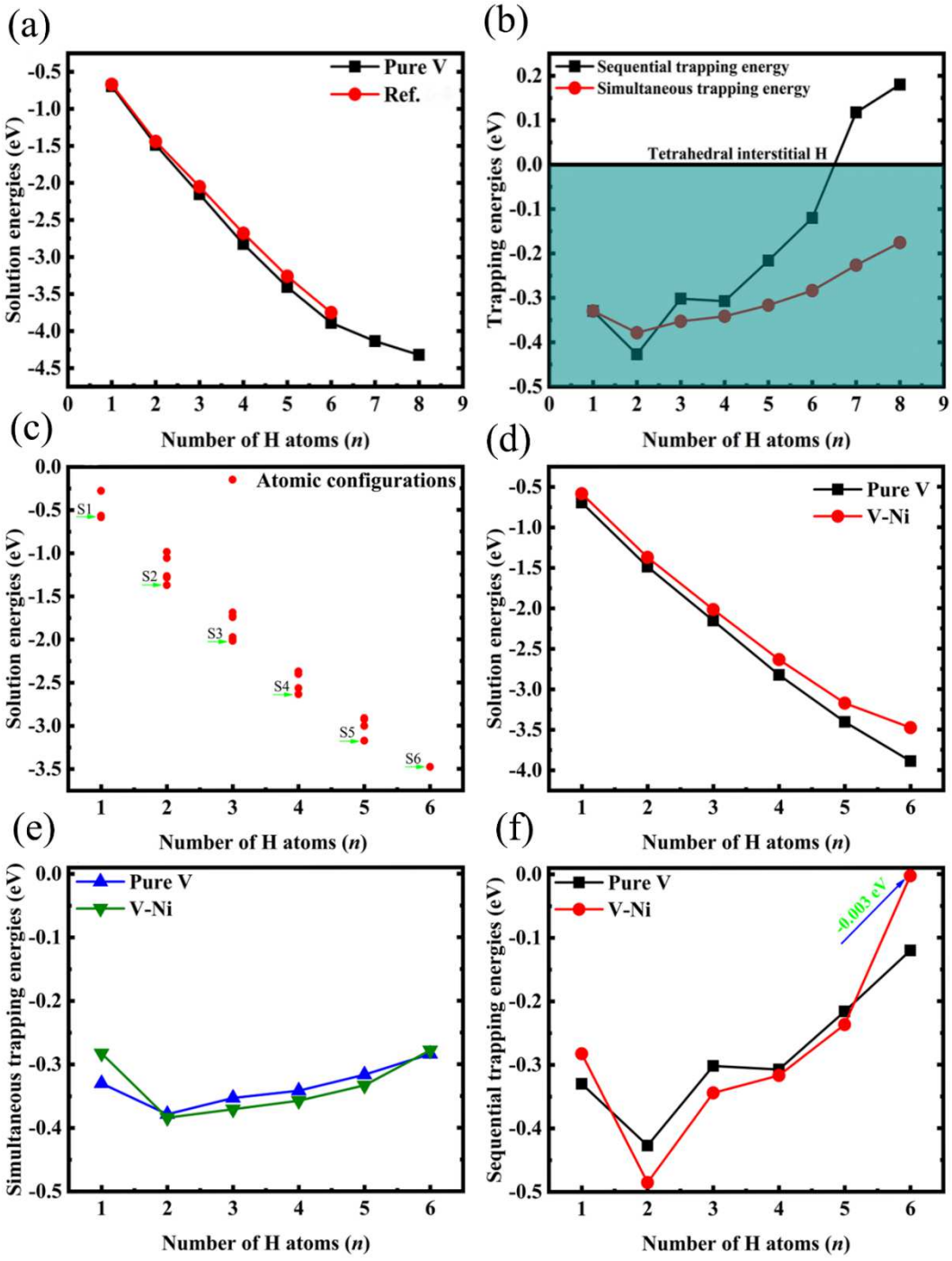

Fig. 6. (a, c, and d) Solution energies and (b, e, and f) trapping energies of multiple H atoms in the monovacancy of V and V–Ni. Reference data are from Pengbo et al. [14].

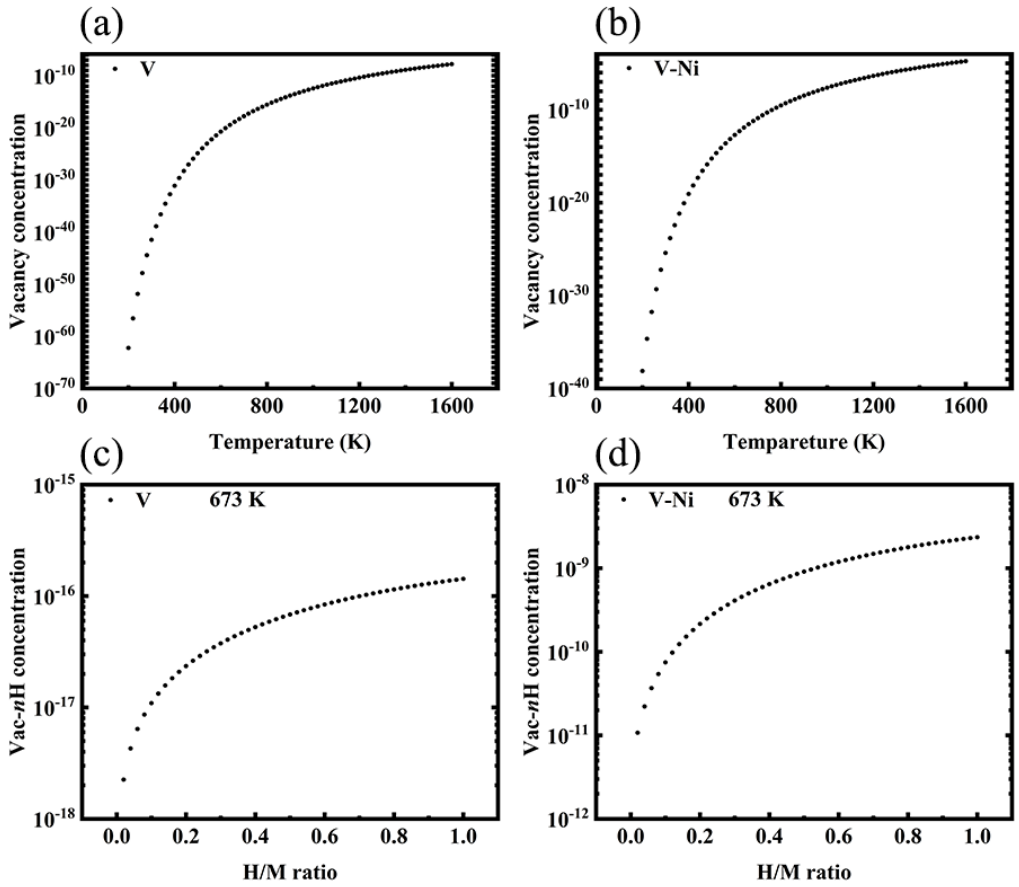

Fig. 7. (a, b) Monovacancy concentration as a function of temperature and (c, d) the functional relationship between the Vac-$\underline{n}$H cluster and H/M rate.

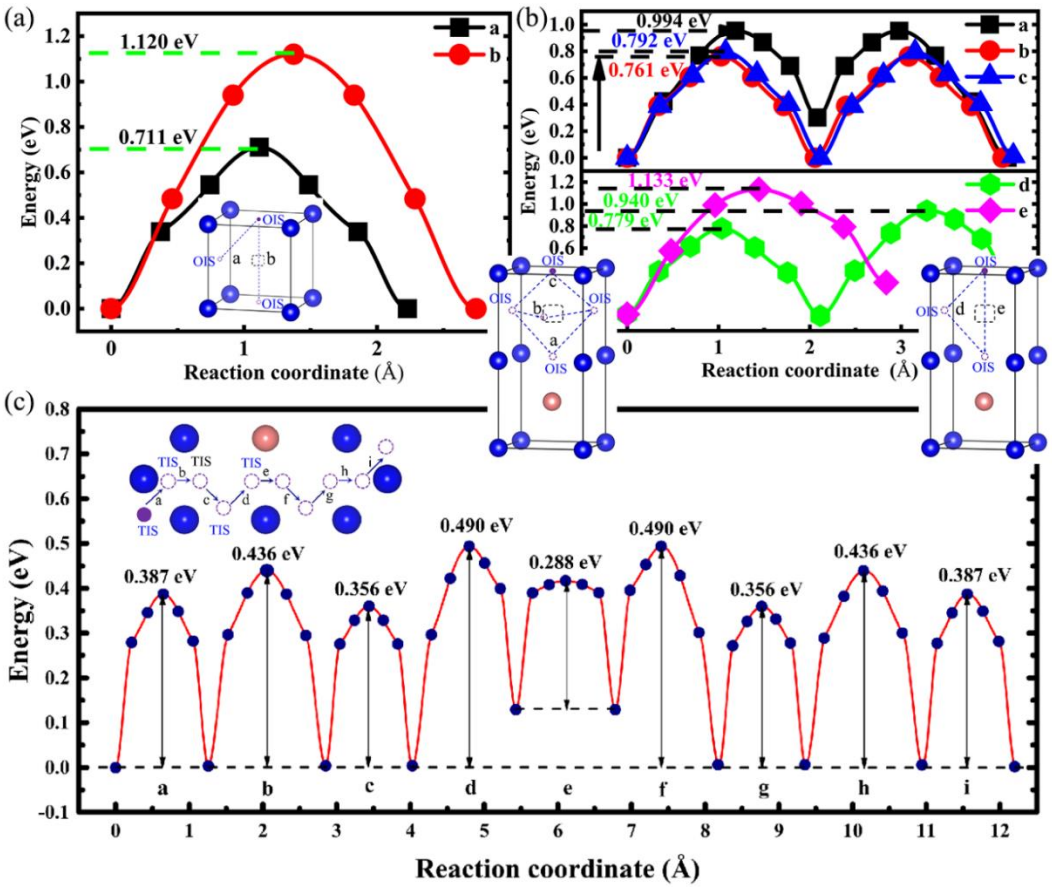

Fig. 8. Diffusion paths and energy barriers for the H atom in (a) V and (b) V–Ni vacancies, and (c) V–Ni interstitials.

Figures

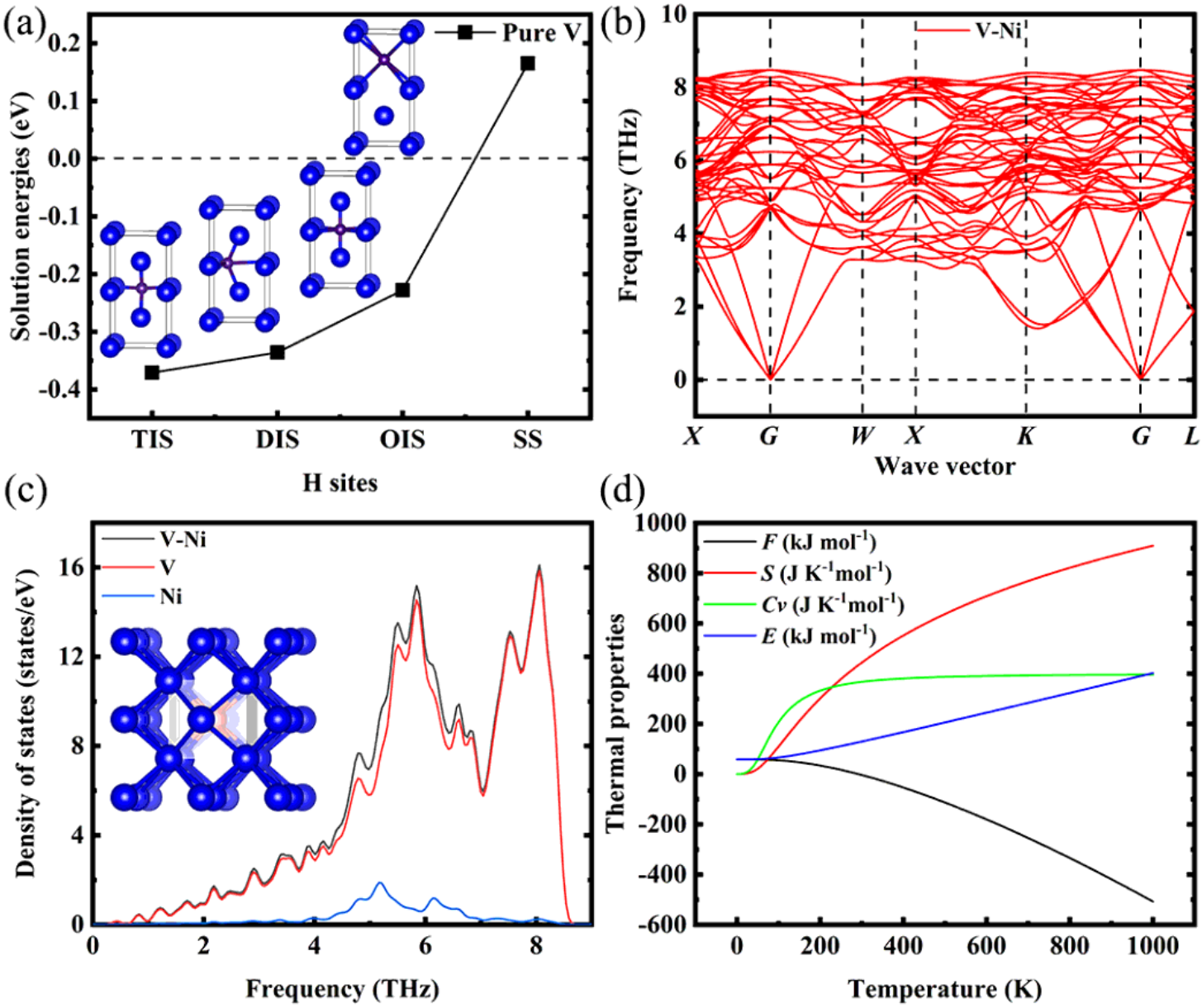

Figure 1

(a) Solution energies of H atoms in interstitial and substitution sites of pure V and (b–d) phonon spectra and thermal properties of V–Ni. The blue, red, and purple spheres denote the V, Ni, and H atoms, respectively.

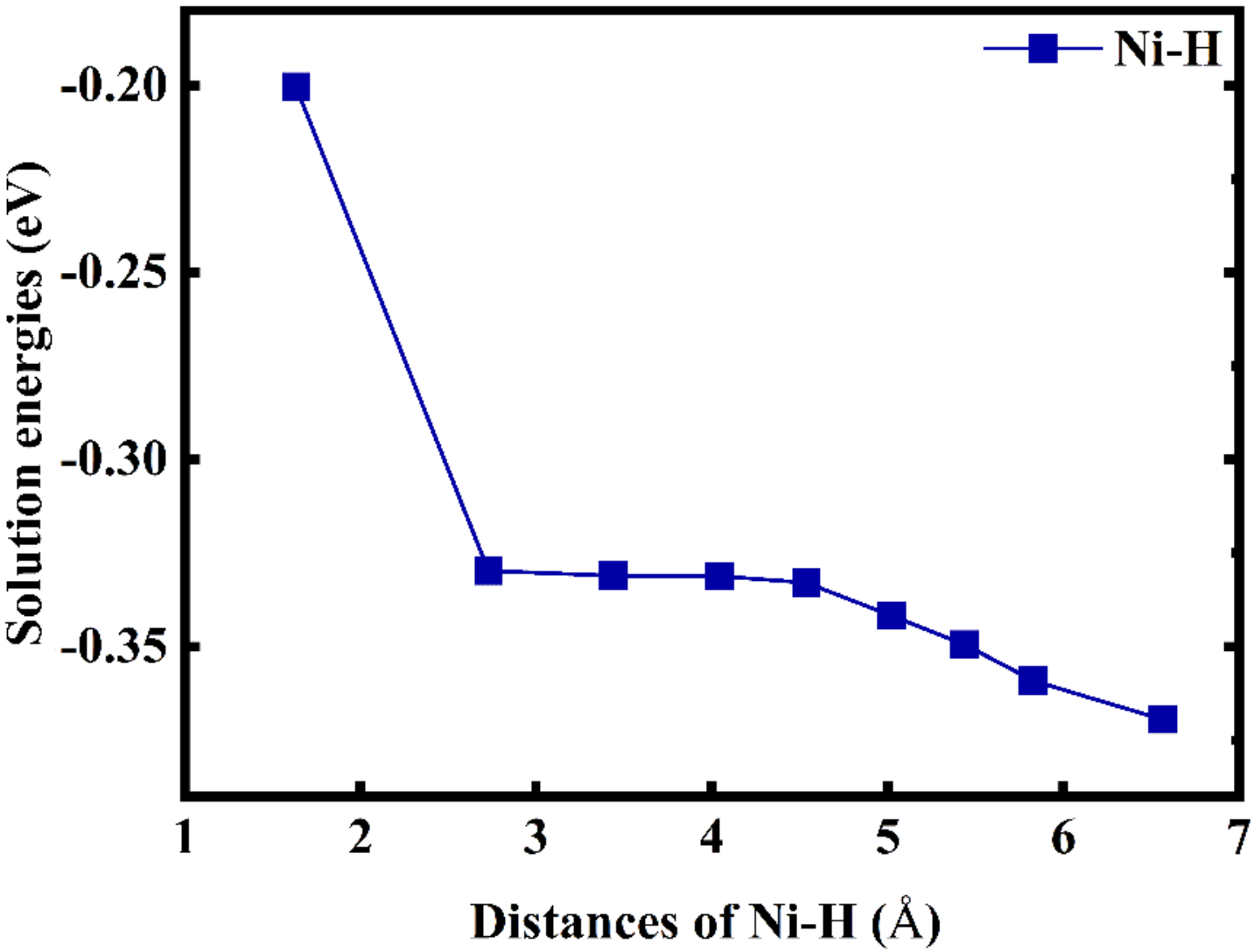

Figure 2

Solution energies of H atoms with respect to the Ni–H distances in the TIS of V–Ni alloys.

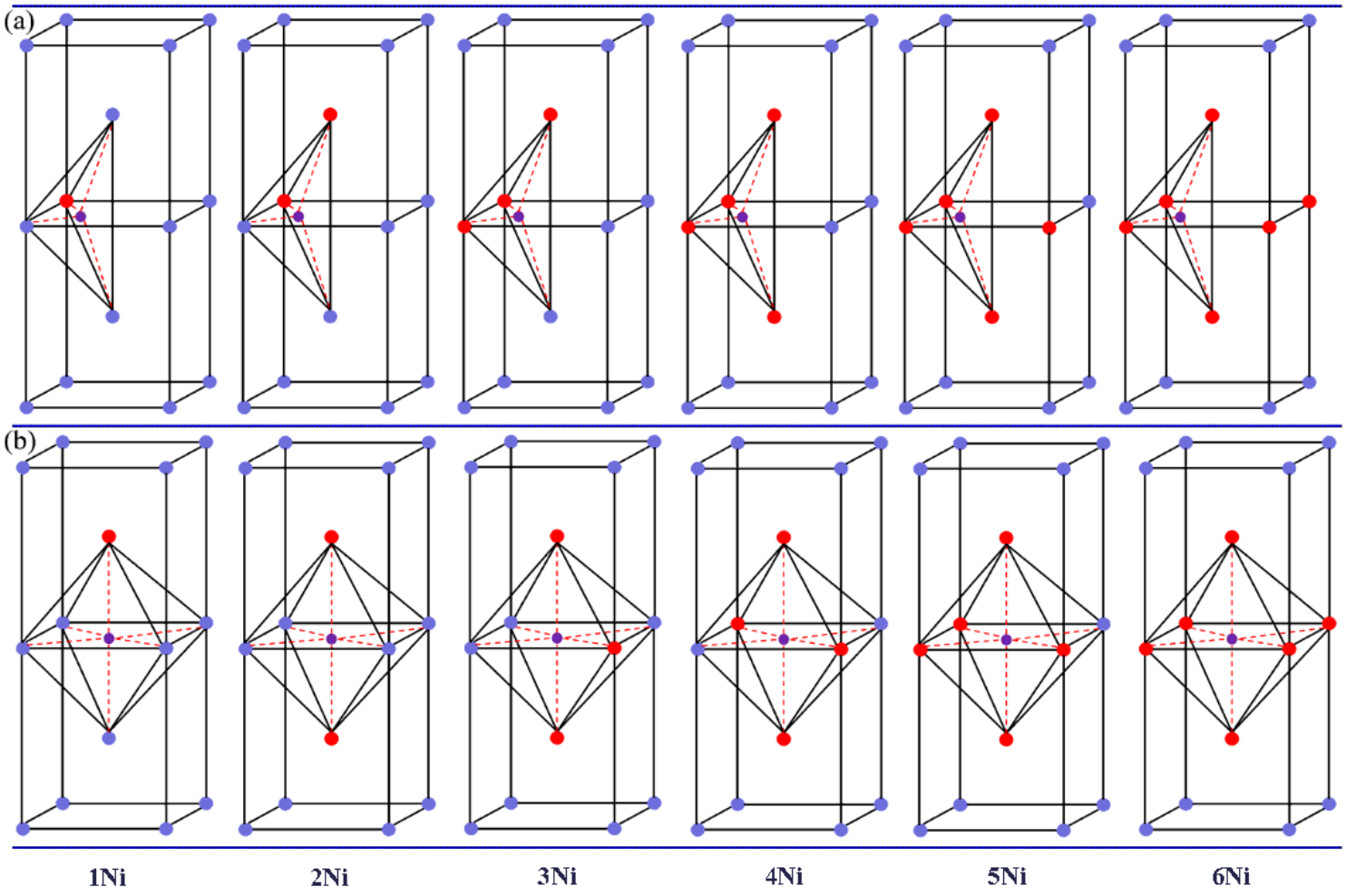

Figure 3

Models demonstrating the substitution of V atoms by different numbers of Ni atoms at the (a) TIS and (b) OIS.

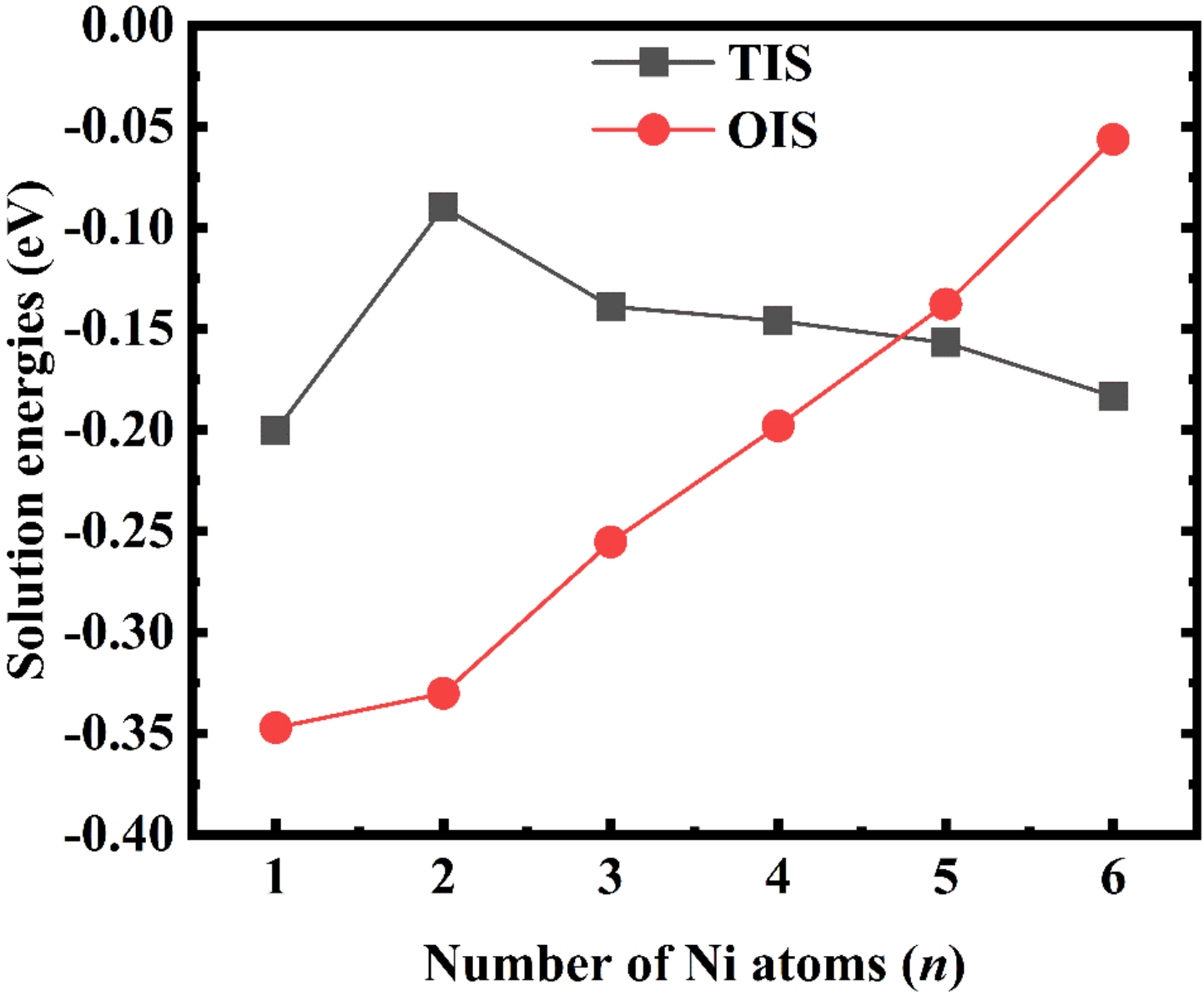

Figure 4

Solution energies of one H atom at the TIS and OIS near (n = 1–6) Ni atoms.

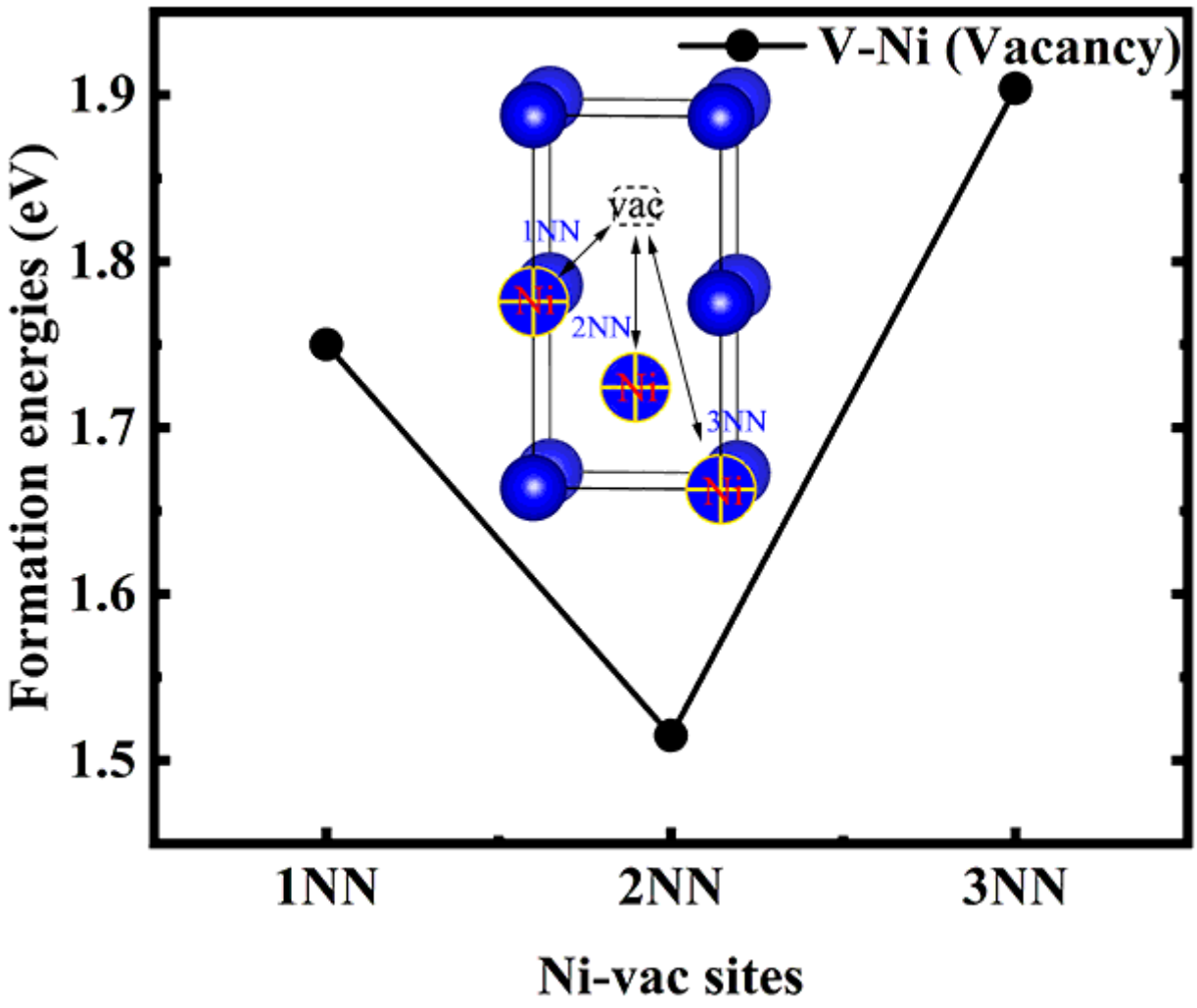

Figure 5

Monovacancy formation energies in the V–Ni alloy.

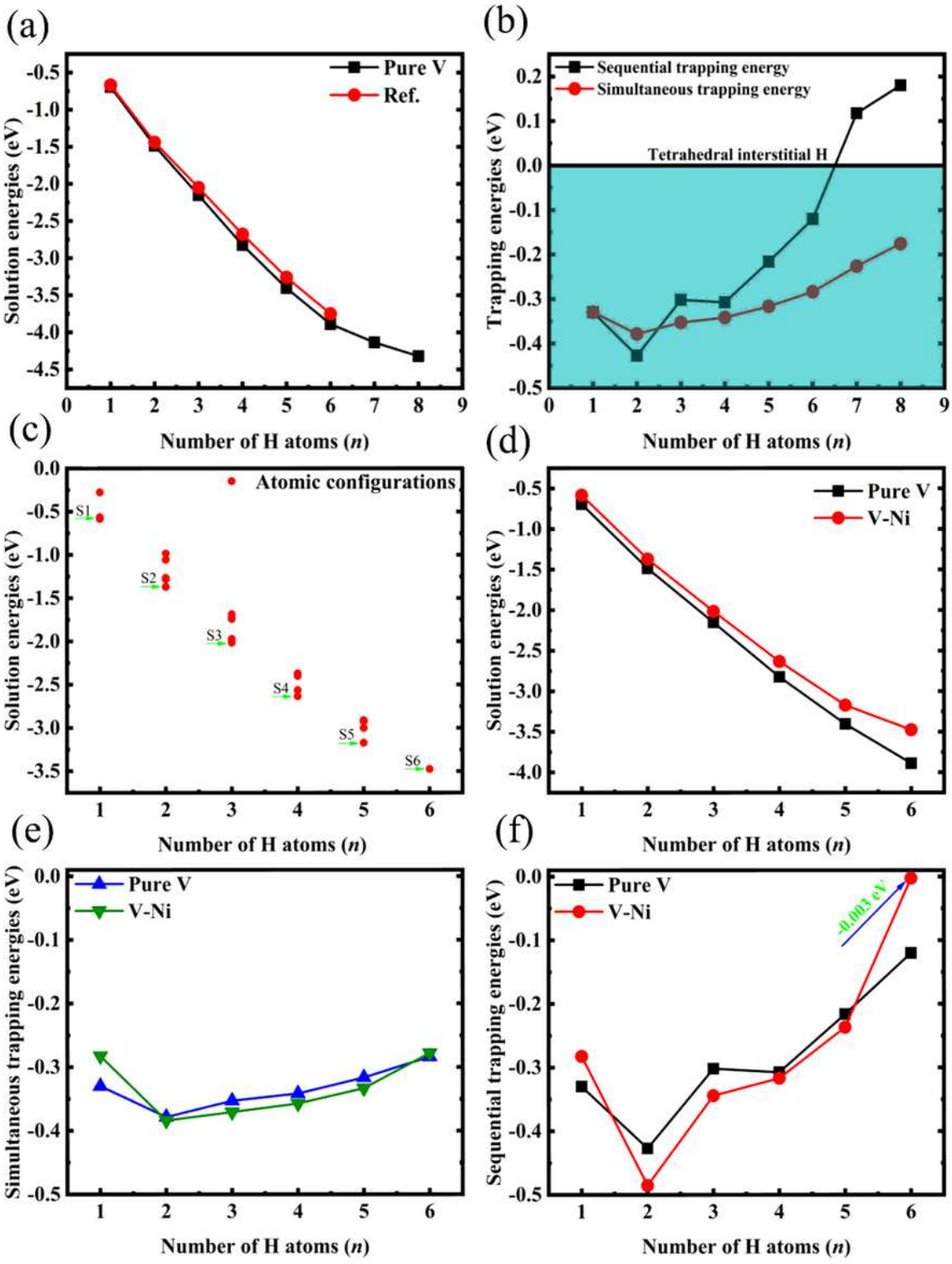

Figure 6

(a, c, and d) Solution energies and (b, e, and f) trapping energies of multiple H atoms in the monovacancy of V and V–Ni. Reference data are from Pengbo et al. [14].

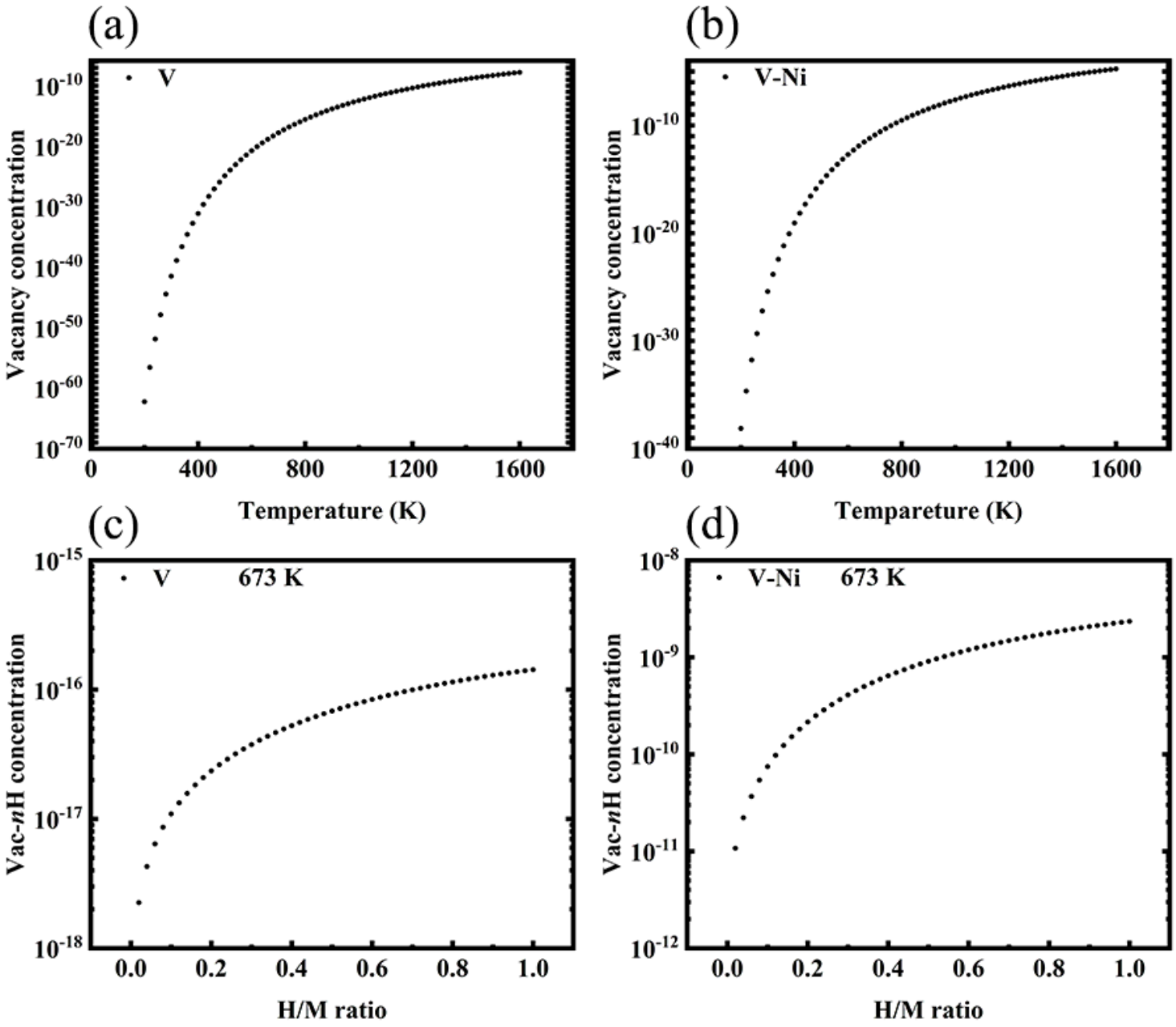

Figure 7

(a, b) Monovacancy concentration as a function of temperature and (c, d) the functional relationship between the Vac-nH cluster and H/M rate.

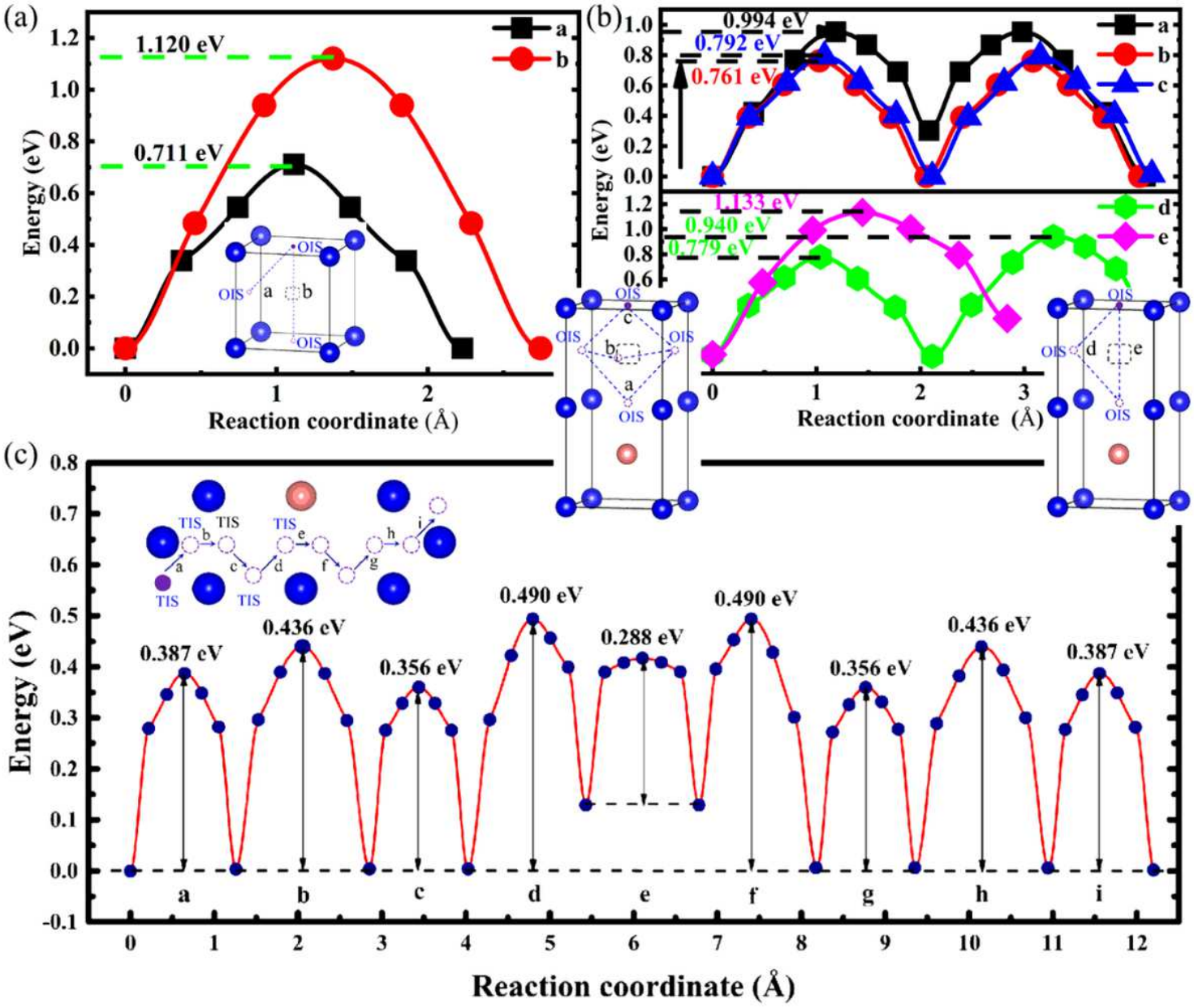

Figure 8

Diffusion paths and energy barriers for the H atom in (a) V and (b) V–Ni vacancies, and (c) V–Ni interstitials.